A Theoretical Study of Imidazole- and Thiol-Based Zinc Binding Groups Relevant to Inhibition of Metzincins

Douglas P. Linder and Kenton R. Rodgers*

Department of Chemistry, Biochemistry, and Molecular Biology, North Dakota State University, Fargo, North Dakota 58105

Received: November 13, 2003; In Final Form: June 28, 2004

In this report, we present a quantum chemical/density functional theory (DFT) study of possible zinc binding modes for five imidazole- and thiol-based ligands relevant to metzincin (MMP and ADAM) inhibitor design. The gas-phase DFT calculations show that, while the imidazole-based ligands may bind zinc in either a five-coordinate bidentate or a four-coordinate monodentate manner, the deprotonated thiolate-containing mercaptoketone and mercapto alcohol ligands are not strongly bidentate, in agreement with recently reported model complex structures. On the basis of modeling of ligand−water exchange reactions, we estimate that the free energy released upon coordination of these zinc binding groups to metzincins decreases in the order mercaptoketone > mercapto alcohol > imidazole-based. The range of binding free energies, however, is only about a few kcal/mol, in the gas phase. In addition, calculated proton dissociation energies show that the driving force for deprotonation of coordinated thiol is greater than that for either imidazole or water. In other words, the Zn−SRH moieties are generally more acidic than their or Zn−ImH or Zn−OH_2 counterparts. These results suggest feasibility of imidazole-based chelating moieties as zinc binding groups in the design of MMP and ADAM inihibitors.

1. Introduction

Zinc-dependent proteases constitute a superfamily of proteolytic enzymes that exhibit an impressively diverse array of functions. The metzincins are a subset of the zinc-dependent proteases and constitute a family of endopeptidases, all of which share a conserved Met in a hydrophobic turn vicinal to the catalytic zinc. Additionally, in its resting state the catalytic zinc is coordinated by the side chains of three conserved His residues and a water molecule. The three conserved His residues occur in the consensus zinc-binding sequence HExxHxxGxxH.[1−3] By virtue of its coordination to the catalytic Zn(II) center, the water molecule is sufficiently nucleophilic to make a facile attack on the scissile peptide bond.[1−3] The metzincins include the matrix metalloproteinases (MMPs) and "a disintegrin and metalloprotease" (ADAMs), which comprise catalytic domains with striking sequence homology and structural homology in their catalytic sites.[3] The metzincins (MMPs and ADAMs) are involved in the degradation and remodeling of the extracellular matrix (ECM) and basement membrane, and in cell−cell signaling.[1,2] The correlation between MMP and ADAM activities and advanced stages of disease has driven the development of MMP and ADAM inhibitors (MMPIs) as therapeutic agents with cancer and arthritis providing much of the impetus.[1−4] However, despite the myriad of MMPIs synthesized to date, none have passed phase III clinical trials for those diseases.[5] Periostat, an oral agent against periodontal disease, is the only FDA approved MMP inhibitor.[6] It is apparent that different approaches are needed for targeting MMPs.[7]

One alternative approach to inhibitor design is based on modification of its zinc binding group (ZBG), which is that part of the inhibitor which directly interacts with the catalytic zinc ion. The largest class of metzincin inhibitors studied so far has been based on the hydroxamic acid ZBG.[3] This binding group is a good chelator of the catalytic zinc ion and inhibitors with sub-nanomolar inhibition constants (K_i's) have been synthesized using this ZBG. One potential problem with using the hydroxamic acid-based inhibitors is that they are also effective chelators of other physiologically important ions, particularly iron.[8] Hence, use of these drugs at inhibitory levels often leads to deleterious physiological side effects. In addition, these inhibitors have shown that compounds with very small K_i's are not necessarily useful as drugs (therapeutics); other factors including solubility, bioavailability, and the pharmacokinetics need to be considered.

As a beginning to novel zinc binding group design, we have synthesized and characterized several tris(2-aminoethyl)amine (tren)-based inhibitors incorporating various imidazolyl and thiazolyl substituents to yield ligands having three pendant bidentate chelating arms, as shown in Figure 1.[9] These tripodal ligands exhibit promising inhibitory properties that suggest the chelating arm structures may be useful ZBGs for further development in the design of pharmaceutical agents. They are straightforward to synthesize in high purity, have reasonable water solubility, and are competitive inhibitors of MMPs-9 and -13[9] with K_i's in the low μM range. Figure 2 shows imine- and secondary amine-based chelating structures found in two of the imidazole-based tripodal inhibitors. In this paper, we present a gas-phase quantum chemical/density functional theory study of the different binding modes for neutral and deprotonated forms of the two ligands shown in Figure 2, when bound to a small molecule model comprising the catalytic zinc center and its protein-based ligands, $[Zn(His)_3]^{2+}$, as found in the active sites of the metzincins. Comparison of the calculated stabilities of ZBG-bound zinc model complexes reported here suggest that the lowest energy structure of the inhibited enzyme active sites

* To whom correspondence should be addressed. Phone: 701-231-8746; fax: 701-231-8831; e-mail: Kent.Rodgers@ndsu.nodak.edu.

10.1021/jp037474f CCC: $27.50
Published on Web 08/18/2004

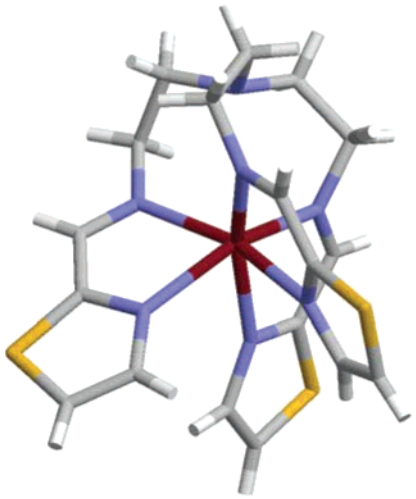

Figure 1. $[Zn(Tatren)]^{2+}$, zinc complex of a thizaole-based tripodal ligand synthesized from 2-thiazolecarboxaldehyde and tris(2-aminoethyl)amine (tren).

L1 L2

Figure 2. Imidazole-based zinc binding groups.

could contain a chelated five-coordinate or a four-coordinate zinc center. Interestingly, the energy differences between four- and five-coordinate zinc centers are often small enough that the lowest energy structure may be dictated by protein environment or solvation effects. The influence of protein environment on the stability of a particular coordination number or geometry at a metal center is, at best, difficult to dissect from the intrinsic tendencies of the structure and, at worst, impossible as the contributions are often not energetically independent. Thus, it seems unlikely that a full understanding of the contribution of ZBG coordination to K_i for the corresponding inhibitor and to the stability of its active site zinc complex will come from a systematic experimental study. The intrinsic stabilities of the coordinated zinc centers can, however, be studied as a function of ZBG properties by computational methods because the mitigating environmental factors can be eliminated by working in the gas phase. This approach provides insight into the intrinsically most stable configuration of the ZBG complex.

One motivation for the study of imidazole-based ZBGs is the prevalence of imidazole (ImH) in biochemical systems. Imidazole from the side chain of His commonly coordinates to zinc in proteins and enzymes, including the metzincins.[10−12] The protonation state of ImH, when coordinated to zinc, has been studied by several groups in recent years.[13,14] Previous theoretical studies have suggested that His can be fully or partially deprotonated, at least when in a Zn(II)-Im---H---Asp/Glu triad.[15] However, whether the ImH proton remains on the zinc-bound ligand or is transferred to a second shell residue depends on several factors including the nature of other first- and second-shell zinc ligands, as well as the solvent accessibility of the zinc center.[13] In fact, calculations have also shown that the $Zn(II)\text{-}ImH^0\text{---}MeCOO^-\text{---}H_2O$ quartet, containing a neutral coordinated imidazole, is energetically more stable than that containing $Zn(II)\text{-}Im^-\text{---}MeCOOH^0\text{---}H_2O$.[16] As it seems clear that the protonation state of imidazole can vary when bound to zinc sites in proteins, we have calculated binding modes for

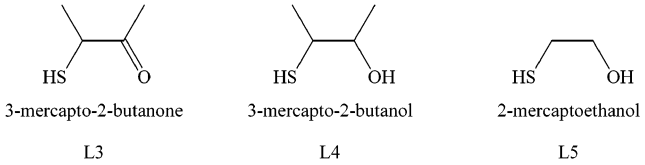

3-mercapto-2-butanone 3-mercapto-2-butanol 2-mercaptoethanol

L3 L4 L5

Figure 3. Thiol-based zinc binding groups.

both the protonated and deprotonated forms of the imidazole-based ligands shown in Figure 2.

In addition to the determination of the zinc binding modes for these novel tren-imidazole based inhibitors of Figure 2, the binding modes for two classes of thiol-based inhibitors, mercaptoketone and mercapto alcohol, are also analyzed using the same computational techniques. The proposed ZBGs for these inhibitors are modeled by the compounds shown in Figure 3. Campbell et al.[17] and Levin et al.[18] have prepared a series of mercaptoketone and mercapto alcohol compounds. On the basis of analysis of binding affinities, they suggest that both classes of inhibitors form bidentate zinc complexes. Recently, Puerta et al.[19] have experimentally determined the binding modes for the small molecule models in Figure 3 and their results show that the binding of the mercaptoketone yields a bidentate structure with a typical Zn−S distance and a long Zn−O distance. In contrast, the two mercapto alcohols coordinate to give monodentate complexes. These binding modes were determined by forming adducts with the zinc complex of (hydrotris(3,5-phenylmethylpyrazoyl)borate), $[ZnTp^{Me,Ph}]$, and examining their structures by X-ray crystallography.[19] This is a promising approach to the design and evaluation of drug−metalloptrotein interactions, as it provides a fast and effective means of assessing these interactions without having to solve the atomic level structure of the inhibited enzymes.[20,21] A potential drawback of this approach is that there seems to be a strong driving force for deprotonation of protic ZBGs in the crystal to yield a neutral complex. Thus, any influence of ZBG protonation on the structure of the zinc complex or its interaction with the enzyme active site cannot be straightforwardly studied by this method. Because computational methods allow investigation of both protonated and deprotonated ZBGs, they are well suited to complement the small-molecule cyrstallographic studies. Additionally, the $Tp^{Me,Ph}$ ligand contains three bulky phenyl groups that form a pocket in which the ZBG must fit. These groups could influence the denticity of the ZBG complex via steric or hydrophobic interactions that are distinct from those in the enzyme active sites and they provide no opportunity for studying the effects of intramolecular H-bonding that characterizes many of the inhibitor complexes of the metzincins.

With the experimentally determined mercaptoketone and mercapto alcohol $ZnTp^{Me,Ph}$ structures in hand, it was possible to compare crystal structures of the model complexes to our calculated structures. In the $ZnTp^{Me,Ph}$ complexes, these thiols crystallize as charge-neutral thiolate complexes. Sulfur coordination to zinc is also quite common in proteins and the consensus is that it generally binds zinc as a thiolate in most cases.[22,23] Therefore, we performed our quantum calculations using the thiolate and alkoxide forms of the structures shown in Figure 3. Our density functional theory calculations reveal only small differences between the calculated $[Zn(ImH)_3ZBG]^+$ and experimental $[ZnTp^{Me,Ph}ZBG]$ binding modes.

The computational approach used in this study is based on the first-principles quantum chemistry method, density functional theory (DFT). Density functional theory and in particular the B3LYP[24] quantum chemical method has proven to be a very useful tool for elucidating first-row transition-metal interactions,

TABLE 1: Gas-Phase Basicities, $-\Delta G_{298K}$ for $B + H^+ \rightarrow BH^+$

	gas-phase basicity (kcal/mol)	
base	B3LYP/6-31+G(d,p)//6-31G(d)	experimental[a]
NH_3	195.8	195.7
pyrazole	205.2	205.7
thiazole	206.2	208.4
imidazole	216.8	217.3

[a] Reference 31.

often providing geometries and energies better than traditional ab initio based correlation methods and at a fraction of their computational cost.[25,26]

2. Computational Methods

The catalytic zinc coordination sphere in all metzincins contains three histidine residues coordinated via their N_ϵ nitrogen atoms. In the inactive zymogens, a cysteine is coordinated to the catalytic zinc center by way of the thiolate S, producing a four-coordinate distorted tetrahedral structure. Upon activation of these enzymes, the Zn−cysteine thiolate is replaced by a catalytic water molecule.[27] In the present calculations, the histidine residues were modeled by neutral imidazole (ImH) ligands and the first coordination sphere is represented by [Zn(II)$(ImH)_3$L], where L is the ligand whose ZBG is being investigated. In this paper, the ZBGs of five ligands were investigated, as shown in Figures 2 and 3. The ligands shown in Figure 2 can be considered as being one arm of the tripodal inhibitor/ligand 4-Imtren/tris[2-(((4-imidazolyl)methylidene)-amino)ethyl]amine, which we designated as L1, and its reduced analogue, L2, while Figure 3 illustrates the three thiol-containing inhibitors investigated by Puerta and co-workers,[19] 3-mercapto-2-butanone (L3), 3-mercapto-2-butanol (L4), and 2-mercapto-ethanol (L5).

All DFT calculations were carried out using the B3LYP[24] hybrid exchange-correlation functional as implemented in the Gaussian 98 program package.[28] All structures were first fully optimized at the B3LYP level of theory using the 6-31G basis set. At these geometries, vibrational frequency calculations were performed to obtain the zero-point energy and to estimate the thermal corrections to the enthalpy, *H*, and entropy, *S*. To further refine the calculated structures, geometry optimizations were then performed with the larger 6-31G(d) basis set (Wachters-Hay for Zn[29]), which has been used successfully by others for similar calculations involving the MMP active site.[30] This level of theory gives a reasonable geometry for the zinc complex of Figure 1 with calculated bond lengths of Zn−N(imine) = 2.199 Å and Zn−N(thiazolyl) = 2.304 Å (in C_3 symmetry), which compare favorably with the average single-crystal bond lengths of Zn−N(imine) = 2.147 Å and Zn−N(thiazolyl) = 2.263 Å. To further improve the energy estimates, single-point B3LYP calculations were then performed with the larger 6-31+G(d,p) basis set (Wachters-Hay for Zn) at the 6-31G(d) geometries. The latter calculations are represented as B3LYP/6-31+G(d,p)//6-31G(d). Unfortunately, accurate energetics for zinc complexes of this ligand family are not available. However, when compared to experimental values, this level of theory provides excellent gas-phase basicities for NH_3, imidazole, thiazole, and pyrazole, as shown in Table 1. For this set of representative compounds, the level of theory used in this study provides an average absolute deviation of only 0.8 kcal/mol from experimental values.

3. Results and Discussion

3.1. Binding Modes. Hereinafter, all of the structures shown are fully optimized B3LYP/6-31G(d) structures, with important distances and bond lengths indicated for the different ligand binding modes. Also shown in these figures are the relative energies (ΔG_{298} and ΔG_0 in kcal/mol) of the different bound structures computed at the B3LYP/6-31+G(d,p)//6-31G(d) level of theory. The frequency calculations for these structures show no imaginary frequencies, indicating true minima on the B3LYP/6-31G potential energy surface. All calculations were run as singlet electronic states and all reported values are in vacuo. Complete Cartesian coordinates for the calculated structures are included as Supporting Information.

3.1.A. Imidazole-Based ZBGs. L1 (Neutral). For all the models studied, there are multiple binding modes possible and nowhere is this more evident than for L1, a diimine-based ligand consisting of 18 atoms in its charge-neutral state. For the [Zn$(ImH)_3$ (L1)]$^{2+}$ complex, a four-coordinate monodentate structure **1** is lowest in energy, as shown in Figure 4. The geometry of **1** has Zn−(L1) coordination in what we refer to as an "end-on" orientation with a slightly distorted tetrahedral arrangement of ligand atoms about Zn wherein ∠N−Zn−N bond angles range from 107.3 to 113.4°, and Zn−N(L1) = 2.00 Å, which is noticeably shorter than the three Zn−N(ImH) bonds. An interesting characteristic of **1** is the formal −1 charge on the imidazole ring and a protonated acyclic imine nitrogen of the L1 ligand. The energy of **1** with the imine-H removed and placed on the L1-imidazole (not shown) is higher by 7.4 kcal/mol. Additionally, the stability of complex **1** is enhanced by the intramolecular (intraligand) H-bond that is not possible in the other isomers shown in Figure 4.

The second most stable neutral L1 isomer, **2**, is five-coordinate and bidentate. The geometry of **2** is best described as distorted trigonal bipyramidal with one ImH N atom and the acyclic imine N atom of L1 occupying the axial positions. The Zn−N bond distances to L1 2.11 Å N(4-ImH) and 2.35 Å N(imine) are significantly longer than those of **1** and show that in the bidentate structure the Zn−imidazole bond is stronger than the Zn−imine bond. The rigid and somewhat sterically demanding five-membered chelate ring has a constrained N−Zn−N angle of 75.2°. This structure, as well as those of all five-coordinate complexes in this report, can be described using the geometric parameter τ.[32] This parameter is an index of the degree of trigonality along the continuum between trigonal bipyramidal and square (rectangular) pyramidal geometries. The value is obtained by dividing the difference between the two largest bond angles in the complex by 60°; $\tau = 1$ for a perfect trigonal bipyramid and $\tau = 0$ for a perfect square pyramid. The τ value for structure **2** is 0.72, indicating a distorted trigonal bipyramidal structure.

Two higher energy four-coordinate, monodentate [Zn$(ImH)_3$-(L1)]$^{2+}$ complexes were located, one N(4-ImH) bound, **3**, and one N(imine) bound, **4**. These structures are 16.4 and 20.6 kcal/mol higher in energy than the ground-state structure, respectively. The geometry of **3** is very close to tetrahedral with ∠N(4-ImH)−Zn−N(ImH) of 109−110°. The Zn−N(4-ImH) bond distance of 2.04 Å is only slightly longer than its counterpart in the ground-state structure, **1**. The geometry of the highest energy isomer, **4**, is best described as distorted tetrahedral with ∠N(imine)−Zn−N(ImH) of 110−112° and a Zn−N(imine) bond length of 2.04 Å, the same as in **3**.

$L1^-$ (Anionic). To produce the anionic form of the L1 ligand, $L1^-$, the N−H proton was removed. Figure 5 shows the four lowest energy [Zn$(ImH)_3$(L1)]$^+$ complexes with **5**, a five-

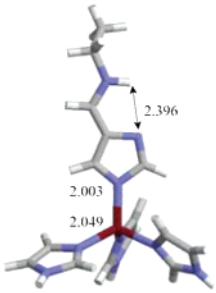

1 (0.0, *0.0*)

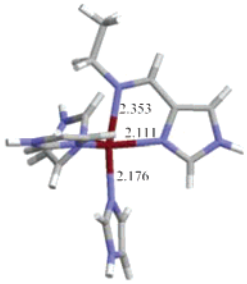

2 (6.6, *4.9*)

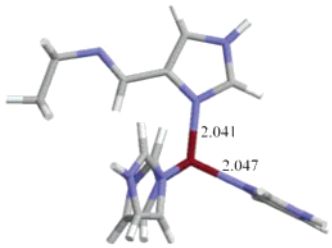

3 (16.4, *14.7*)

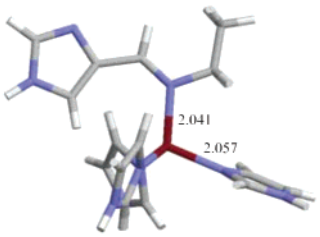

4 (20.6, *19.4*)

Figure 4. $[Zn(ImH)_3(L1)]^{2+}$. B3LYP/6-31+G(d,p)//6-31G(d) relative energies for the neutral-L1 zinc complex (ΔG_{298} and ΔG_0 in kcal/mol).

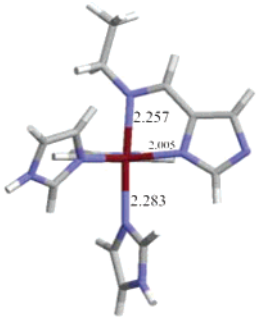

5 (0.0, *0.0*)

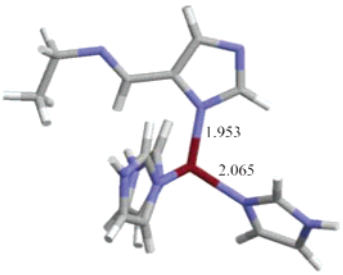

6 (9.7, *11.5*)

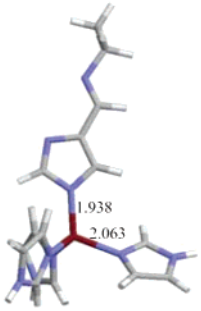

7 (11.7, *14.0*)

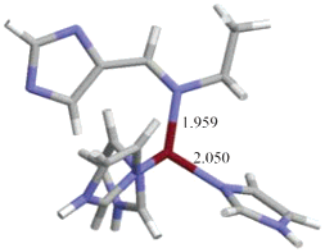

8 (27.2) [6-31G]

Figure 5. $[Zn(ImH)_3(L1)]^{+}$. B3LYP/6-31+G(d,p)//6-31G(d) relative energies for the anionic $L1^-$ zinc complex (ΔG_{298} and ΔG_0 in kcal/mol).

coordinate chelated complex, being the lowest energy isomer. This is not surprising since single-crystal X-ray structures show that the Zn(II) complex of a tripodal thiazole-containing analogue of L1, Tatren (Figure 1), chelates Zn(II) in a similar manner using these two nitrogen atoms.[9] The geometry of **5** is trigonal bipyramid about Zn with the acyclic imine N of $L1^-$ and a N atom from an ImH ligand occupying the axial positions, both with noticeably longer bonds than their equatorial counterparts. The τ value for **5** is 0.83 which indicates modest trigonal distortion with the $\angle$N(imine)−Zn−N(4-Im) angle of 80.2° being slightly distorted from the idealized trigonal bipyramid angle of 90.0°.

All the four-coordinate $[Zn(ImH)_3(L1)]^{+}$ isomers, **6**−**8**, are significantly higher in energy (≥9.7 kcal/mol) than **5**. All exhibit tetrahedral coordination geometries and contain relatively short Zn−N($L1^-$) bonds of 1.94−1.96 Å, which is ∼0.05 Å shorter than their neutral L1 analogues.

Instead of deprotonating the L1 ligand through its imidazole ring, the question may be asked is it energetically more favorable to deprotonate one of the ImH side chains coordinated to the catalytic zinc in the protein? To address this question, we have deprotonated one of the three ImH rings starting from the two lowest energy $[Zn(ImH)_3(L1)]^{2+}$ structures, **1** and **2**. Energetically, the end-on isomer containing a deprotonated Im^- and a neutral L1 ligand lies 2.7 kcal/mol higher in energy than **5**, that is, the end-on isomer prefers to have a neutral ligand and a deprotonated Im^- rather than vice versa. However, deprotonating the bidentate structure **2** in the axial ImH position produces a structure that is 7.0 kcal/mol higher than **5**, which indicates that the bidentate singly charged L1 complex is most stable when the chelating ligand is deprotonated. Both the 2.7 and 7.0 kcal/mol differences are ΔD_e values from B3LYP/6-31+G(d,p)//6-

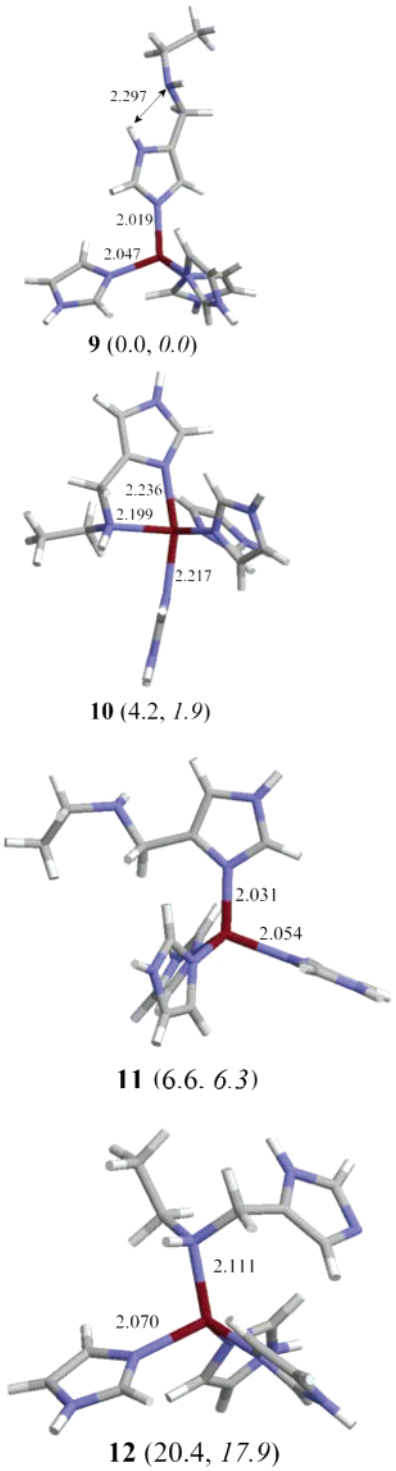

Figure 6. $[Zn(ImH)_3(L2)]^{2+}$. B3LYP/6-31+G(d,p)//6-31G(d) relative energies for the neutral L2 zinc complex (ΔG_{298} and ΔG_0 in kcal/mol).

31G(d) calculations; in other words, neither accounts for zero-point energy or availability of thermal energy. Overall, these results suggest that, at least in the gas phase, it is energetically more favorable to deprotonate the ZBG imidazole than the imidazole of an endogenous histidine.

L2 (Neutral). Figure 6 shows the four lowest energy isomers/tautomers of the 48 atom $[Zn(ImH)_3(L2)]^{2+}$ system, **9**−**12**. As in the neutral L1 systems, the lowest energy L2 complex, **9**, is four-coordinate. The bound ligand in **9** is a tautomer of the ligand structure shown in Figure 2, and the L2 is in the end-on orientation. The geometry is slightly distorted tetrahedral with ∠N(4-ImH)−Zn−N(ImH) ≈ 111°, and a Zn−N(4-ImH) bond distance of 2.02 Å, which is slightly shorter than all the Zn−N(ImH) bond lengths of 2.04−2.05 Å. As in **1**, there is an intramolecular H-bond in this complex providing additional stability.

Several five-coordinate, chelated isomers were also located. The lowest energy structure of this group is **10**. This structure is only 4.2 ($\Delta G_0 = 1.9$) kcal/mol higher in energy than the ground state. The topography of **10** is a severely distorted trigonal bipyramid ($\tau = 0.68$) with one N(ImH) and the N(4-ImH) occupying the axial positions; this geometric arrangement is in contrast to the other five-coordinate structures, **2** and **5**, in which the N(4-ImH) atom occupies an equatorial position. The Zn−N(4-ImH) bond distance of 2.24 Å is slightly longer than the equatorial Zn−N(amine) distance of 2.20 Å.

The other two four-coordinate structures, **11** and **12**, are higher in energy than **9** by 6.6 and 20.4 kcal/mol, respectively. The structure with the N(4-ImH) bound **11** is very nearly tetrahedral with ∠N(4-ImH)−Zn−N(ImH) bond angles all close to 109° and a Zn−N(4-ImH) bond length of 2.03 Å, slightly shorter than the Zn−N(ImH) bond distances of 2.04−2.05 Å. The geometry of the highest energy structure, **12**, is very distorted tetrahedral about Zn with N(amine)−Zn−N(ImH) bond angles ranging from 103 to 119 E. The Zn−N(amine) bond length of 2.11 Å in **12** is significantly greater than in the other four-coordinate structures, and shorter than the internal Zn−N(ImH) bonds.

$L2^-$ (Anionic). The anionic form of the L2 ligand, $L2^-$, was formed by removing the imidazole NH proton. Figure 7 shows the three lowest energy $[Zn(ImH)_3(L2)]^+$ complexes. Interestingly, all three structures are close in energy. The four-coordinate end-on structure, **13**, and the five-coordinate chelated structure, **14**, have about equal 0 K energies. However, thermal effects lower the relative energy of the end-on structure significantly, rendering it the ground-state structure.

The geometry of **13** is tetrahedral about Zn with ∠N(4-Im)−Zn−N(ImH) between 109° and 113°. The Zn−N(4-Im) bond length of 1.94 Å is shorter than in the end-on neutral complexes, **1** and **9**, but the same as in the analogous end-on $L1^-$ complex, **7**. Additionally, **13** has an intra-L2 H-bond that likely accounts for the stability of the four-coordinate structure. The input structure for the calculation of **13** had H^+ removed from secondary amine N atom of L2 to yield the corresponding amide. However, the proton transferred from N(4-ImH) to N(amide) during the geometry optimization. Hence, we conclude that the amide lies significantly higher in energy than the ground state and this was our only attempt to locate an amide complex.

The very low energy five-coordinate structure of **14** is best described as a distorted rectangular pyramid with $\tau = 0.24$. In **14**, both L2 nitrogen atoms occupy equatorial positions and an ImH is in the apical position. The highest energy structure, **15**, is four-coordinate and tetrahedral with a Zn−N(4-Im) bond length of 1.95 Å, 0.08 Å shorter than in its neutral counterpart. A four-coordinate Zn−N(amine) structure could not be located; during the geometry optimization, a five-coordinate structure was found.

3.1.B. Sulfur-Containing ZBGs. $L3^-$ (Anionic). Figure 8 shows the two $[Zn(ImH)_3(L3)]^+$ complexes located. The lowest energy structure, **16**, is five-coordinate with a long Zn−O distance, as shown in Figure 8. The geometry of this structure is best described as highly distorted trigonal bipyramidal ($\tau = 0.65$) with the O atom and a N(ImH) atom in the axial positions. The long Zn−O bond is 2.51 Å, while the equatorial Zn−S bond length is shorter at 2.29 Å. Although the Zn−O distance

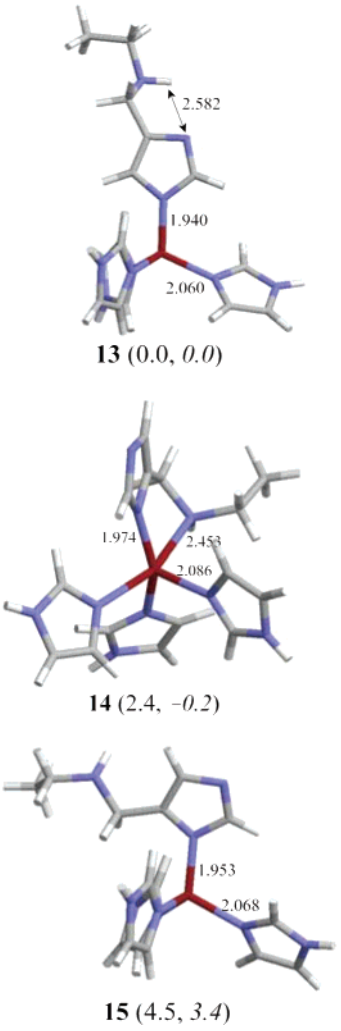

Figure 7. $[Zn(ImH)_3(L2)]^+$. B3LYP/6-31+G(d,p)//6-31G(d) relative energies for the anionic $L2^-$ zinc complex (ΔG_{298} and ΔG_0 in kcal/mol).

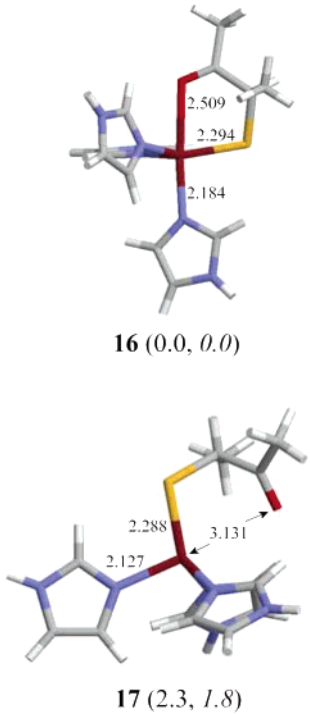

Figure 8. $[Zn(ImH)_3(L3)]^+$. B3LYP/6-31+G(d,p)//6-31G(d) relative energies for the anionic $L3^-$ zinc complex (ΔG_{298} and ΔG_0 in kcal/mol).

is quite long, it is significantly shorter than the sum of the Zn and O van der Waals radii (2.90 Å). Moreover, this structure has significant trigonal bipyramidal character. Taken together, these aspects of the structure have led us to designate it as five- rather than four-coordinate. Although the geometry of **16** is similar to that reported by Puerta et al.[19] for $[ZnTp^{Me,Ph}(L3)]$, their experimental Zn−O distance of 2.33 Å is shorter than our calculated distance but still longer than the experimental Zn−S distance of 2.27 Å, which is comparable to our calculated value.

A four-coordinate S-bound structure, **17**, was located and is close in energy to the ground state at +2.3 ($\Delta G_0 = 1.8$) kcal/mol, Figure 8. This structure has a very distorted tetrahedral geometry with ∠S−Zn−N(ImH) of 103°, 118°, and 125°, a Zn−S bond length of 2.29 Å, and a Zn−O distance of 3.13 Å that is 0.62 Å longer than in **16**. In addition, while the Zn−O distance is too long to suggest any significant bonding interaction, an electrostatic interaction is apparent from the very distorted tetrahedral geometry. A four-coordinate O-bound structure was not found.

$L4^-$ (Anionic). Figure 9 shows four structures located for the 43 atom $[Zn(ImH)_3(L4)]^+$ complex. The lowest energy isomer, **18**, can be described as either weakly five-coordinate or highly distorted four-coordinate S-bound with the Zn−S bond length of 2.27 Å and a long Zn−O distance of 2.72 Å. The geometry of **18** does resemble a five-coordinate distorted trigonal bipyramid ($\tau = 0.69$) more closely than rectangular pyramidal or four-coordinate tetrahedral, with O and N(ImH) atoms in axial positions. The X-ray structure of $[ZnTp^{Me,Ph}(L4)]$ is clearly four-coordinate with a Zn−S bond length of 2.23 Å and a Zn−O distance >4.5 Å.[19]

The second lowest energy structure located, **19**, is only 1.3 kcal/mol higher in energy than **18**. The geometry of **19** is five-coordinate with a τ value of 0.47, indicating a structure about halfway between trigonal bipyramidal and rectangular pyramidal. The Zn−O and Zn−S distances to $L4^-$ are the longest bonds in this structure with the Zn−S bond length of 2.28 Å again being shorter than the long Zn−O distance of 2.58 Å.

A true four-coordinate S-bound $[Zn(ImH)_3(L4)]^+$ complex was located and is shown as **20** in Figure 9. This structure is 5.3 ($\Delta G_0 = +6.6$) kcal/mol higher in energy than **18** but bears the closest resemblance to the X-ray structure of $[ZnTp^{Me,Ph}(L4)]$.[19] The geometry of **20** is best described as severely distorted tetrahedral with ∠S−Zn−N(ImH) bond angles of 107°, 115°, and 122°. The Zn−S distance is relatively short at 2.25 Å and the Zn−O distance of 5.73 Å is nonbonded.

The highest energy isomer, **21**, lies significantly higher in energy than the ground state at +14.2 ($\Delta G_0 = 14.8$) kcal/mol. It is four-coordinate but $L4^-$ is oxygen bound with a short 1.87 Å Zn−O bond. The geometry optimization of **21** began with the four-coordinate Zn−OH···S^- structure, however, the −OH proton transferred to the thiolate S, producing a tetrahedral Zn−O···HS complex with an intramolecular hydrogen bond, ZnO···HS, of length 2.20 Å.

$L5^-$ (Anionic). Three $[Zn(ImH)_3(L5)]^+$ complexes were found and are shown in Figure 10. As in the $L4^-$ complex, the lowest energy $L5^-$ complex, **22** ($\tau = 0.48$), can be described as either very weakly five-coordinate or four-coordinate S-bound, with a long Zn−O distance of 2.76 Å and a normal Zn−S bond length of 2.28 Å. A five-coordinate complex having a shorter Zn−O bond as in **19** was not found, even by optimizing the structure of **19** after replacing its methyl groups by hydrogen

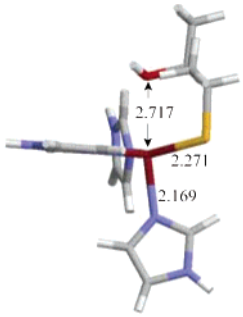

18 (0.0, *0.0*)

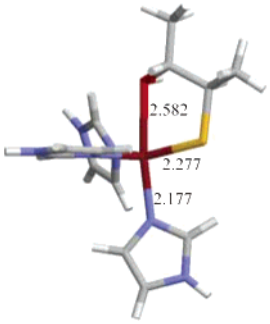

19 (1.3, *1.2*)

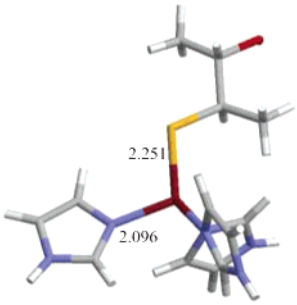

20 (5.3, *6.6*)

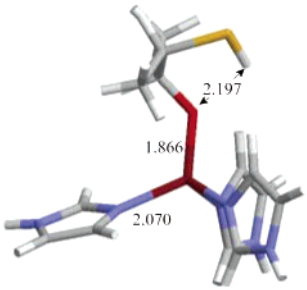

21 (14.2, *14.8*)

Figure 9. $[Zn(ImH)_3(L4)]^+$. B3LYP/6-31+G(d,p)//6-31G(d) relative energies for the anionic-$L4^-$ zinc complex (ΔG_{298} and ΔG_0 in kcal/mol).

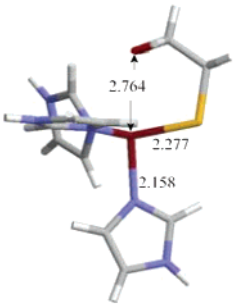

22 (0.0, *0.0*)

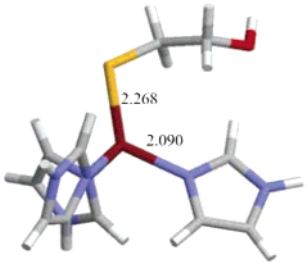

23 (0.3, *0.9*)

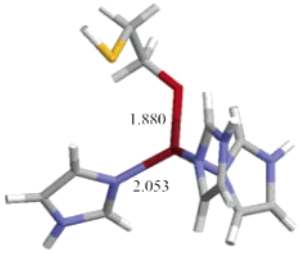

24 (6.7, 7.0)

Figure 10. $[Zn(ImH)_3(L5)]^+$. B3LYP/6-31+G(d,p)//6-31G(d) relative energies for the anionic $L5^-$ zinc complex (ΔG_{298} and ΔG_0 in kcal/mol).

atoms. This result is consitent with the crystal structure of $[ZnTp^{Me,Ph}(L5)]$, which is clearly four-coordinate, having a Zn−S bond length of 2.23 Å and a Zn−O distance of 5.68 Å.[19]

The lowest energy purely four-coordinate S-bound structure (Figure 10 **23**) was located at only 0.3 ($\Delta G_0 = 0.9$) kcal/mol above the ground state. This structure is distorted tetrahedral with ∠S−Zn−N(ImH) of 107°, 113°, and 124°, a Zn−S bond length of 2.27 Å, and a nonbonded Zn−O distance of 4.59 Å. Using a starting structure having atomic coordinates similar to the published X-ray parameters, the resulting optimized structure was four-coordinate and about 1 kcal/mol higher in energy than **23**.

The highest energy $[Zn(ImH)_3(L5)]^+$ complex located in this calculation, **24**, is a four-coordinate O-bound structure that lies 6.7 ($\Delta G_o = 7.0$) kcal/mol higher in energy than **22**. The atomic arrangement of this structure is actually Zn−OG···HS not Zn−OH···S^- and contains a short 1.88 Å Zn−O bond, which is similar to that calculated for the analogous $[Zn(ImH)_3(L4)]^+$ complex, **21**.

3.1.C. Implications for Binding to Metzincin Catalytic Zinc Centers. Figures 4−10 illustrate the intrinsically most stable structures resulting from the binding of a ligand, $L^{0,1-}$, to $[Zn(His)_3]^{2+}$, the generalized and coordinatively unsaturated metzincin catalytic center. In other words, they do not reflect influences of the protein environment. Protein structure and dynamics, as well as changes in solvation energies, and electronic effects of other functional groups are likely to influence the coordination number and geometry of the ZBG-bound catalytic centers. These influences are expected to be slightly different among the 26 or so MMPs, the ADAMs, and other proteins with $[Zn(His)_3]^{2+}$ based active sites and will likely have to be addressed on a case-by-case basis. This is likely to contribute to a better understanding of individual enzymes but will come at a much greater computational cost. However, the vast majority of metzincin inhibitors have some sort of

functionality designed to coordinate or chelate the catalytic zinc binding group.

From analysis of the imidazole-based complexes with neutral L1 or L2 ZBGs, the most stable structures are four-coordinate, tetrahedral, and in the end-on orientation. Four-coordinate tetrahedral Zn geometries are prevalent in protein structures, so this result is not necessarily surprising.[11,12] However, our calculations show that the five-coordinate chelated structures **2** and **10** are only 4.9 and 1.9 kcal/mol higher in energy than the ground state, an energy cost that could easily be born by the formation of nonbonded interactions with and within the enzyme active site. Additionally, it is apparent that both the four-coordinate end-on structures are stabilized by a single intramolecular hydrogen bond as shown in structures **1** and **9**. Thus, it is reasonable to suggest that formation of two or more hydrogen bonds between the inhibitor and the enzyme could invert the energy ordering of **1** and **2**, and **9** and **10**. So, the availability of H-bond donors and acceptors in and around the active site are expected to have a significant influence on the coordination number of the inhibited active site. However, steric crowding around the catalytic zinc center could destabilize the five-coordinate complex in the enzyme active site. For the anionic $L1^-$ and $L2^-$ ligands, the intrinsically most stable structures are the five-coordinate chelates. However for $L2^-$, the four-coordinate end-on mode is favored over the five-coordinate chelated structure if the effect of temperature on binding free energy is taken into account. Therefore, in an environment where nonbonded interactions of the ligand are possbile, both orientations are energetically accessible. This is not so for the anionic $L1^-$ ligand in which the chelated structure is significantly more stable than the four-coordinate end-on structure. For both L1 and L2, the four-coordinate Zn−N(acyclic) structures are quite high in energy, leading us to conclude that this mode of binding is less likely.

From analysis of the different binding modes for the mercaptoketone and mercapto alcohol ligands (**16**−**24**), it seems quite evident that none are expected to exhibit strong bidentate coordination in the metzincin catalytic sites. This is consistent with the X-ray structures for the charge-neutral $[ZnTp^{Me,Ph}L]$ complexes of Puerta et al.[19] Our calculations show that the favored binding mode for $L3^-$ is weakly five-coordinate with a typical Zn−S bond distance and a weak bond between zinc and the carbonyl O atom. This result is also in agreement with the X-ray crystallography results.[19] Our calculations show that the most stable mercapto alcohol structures are very weakly five-coordinate, with long Zn−O distances (bonds) of 2.7−2.8 Å, but with significantly distorted trigonal bipyramidal geometries. However, $L5^-$ exhibits a very low-lying, four-coordinate, and thiolate-bound structure. The experimental structures of the neutral $[ZnTp^{Me,Ph}$(mercapto alcohol)] complexes are also clearly four-coordinate and thiolate-bound.[19] Our DFT results show that the lowest energy $[Zn(ImH)_3$(mercapto alcohol)$]^+$ structures have weak electrostatic interactions between the zinc and oxygen atoms, adding extra stability to these complexes. This electrostatic interaction is not seen in the $[ZnTp^{Me,Ph}$(mercapto alcohol)] crystal structures. At this point, the basis for these small differences between the experimental $[ZnTp^{Me,Ph}$(mercapto alcohol)] structures[19] and our calculated $[Zn(ImH)_3$(mercapto alcohol)$]^+$ structures is not clear. However, they may be attributable to the differences in the charges of the ImH and $Tp^{Me,Ph}$ complexes. Calculations on the neutral $[ZnTp^{Me,Ph}L]$ complexes may shed light on these differences but, with the overall goal of inhibitor/ZBG design, this may or may not yield direct insight toward that goal.

TABLE 2: Relative Free Energies of Ligand Exchange for Reactions 2−11[c]

ligand	rxn	relative ΔG_{0K}	relative $\Delta G_{298\,K}$
		neutral ligands[a]	
L1	2	−23.8	−19.2
L2	4	−30.9	−29.3
L6	11	−20.5	−18.0
CH_3SH	10	0.0	0.0
		anionic ligands[b]	
$L1^-$	3	9.5	12.7
$L2^-$	5	12.8	16.6
$L3^-$	6	4.0	7.6
$L4^-$	7	7.7	10.3
$L5^-$	8	8.4	10.9
CH_3S^-	9	0.0	0.0

[a] Relative to CH_3SH; $\Delta G_{0K} = -1.1$ kcal/mol, $\Delta G_{298K} = 0.6$ kcal/mol. [b] Relative to CH_3S^-; $\Delta G_{0K} = -180.0$ kcal/mol, $\Delta G_{298K} = -178.8$ kcal/mol. [c] Energies are based on B3LYP/6-31+G(d,p)//6-31G(d) calculations and are given in kcal/mol.

3.2. Thermodynamic Parameters. With the ligand (ZBG) binding modes and their relative energies established, we proceed to assess the relative binding affinities of the same ZBGs using the ligand−water exchange reaction represented generically by

$$[Zn(ImH)_3\,OH_2]^{2+} + Ligand^{(0,1)-} \rightarrow [Zn(ImH)_3\,Ligand]^{(2,1)+} + H_2O \qquad \Delta G_{exch} \quad (1)$$

The energy change (ΔG_{exch}) for reaction 1 reflects the relative affinities of $[Zn(ImH)_3]^{2+}$ for the ligand and the catalytic water molecule. This approach has been used previously by Cheng et al.[33] in their theoretical study on the interactions of various anionic zinc binding groups with the catalytic Zn^{2+} ion in matrix metalloproteases. In that study, the correlation between calculated gas-phase binding free energies and in vitro inhibition constants (K_i's) for a series of indolactam-based inhibitors with the two MMPs matrilysin and human fibroblast collagenase was very good.[33] The inhibitors in this study have the same skeleton structure but different ZBGs. The single exception to their ΔG_{exch}, K_i correlation was for an inhibitor with an additional large substituent (an S1′ substituent) near the ZBG (i.e., a quinoline derivative of hypophosphite was being modeled with hypophosphite). Therefore, we would expect our calculated trends in binding affinity to correlate well with in vitro binding affinities for at least the anionic ligands of this study.

Table 2 lists the relative free energies of ligand exchange for reactions 2−11, where the $[Zn(ImH)_3L]^{2,1+}$ energy is that of the ground state for each complex (Figures 4−10).

$$[Zn(ImH)_3(OH_2)]^{2+} + L1 \rightarrow H_2O + [Zn(ImH)_3(L1)]^{2+} \quad (2)$$

$$[Zn(ImH)_3(OH_2)]^{2+} + L1^- \rightarrow H_2O + [Zn(ImH)_3(L1)]^{+} \quad (3)$$

$$[Zn(ImH)_3\,(OH_2)]^{2+} + L2 \rightarrow H_2O + [Zn(ImH)_3(L2)]^{2+} \quad (4)$$

$$[Zn(ImH)_3(OH_2)]^{2+} + L2^- \rightarrow H_2O + [Zn(ImH)_3(L2)]^{+} \quad (5)$$

$$[Zn(ImH)_3(OH_2)]^{2+} + L3^- \rightarrow H_2O + [Zn(ImH)_3(L3)]^{+} \quad (6)$$

$$[Zn(ImH)_3(OH_2)]^{2+} + L4^- \rightarrow H_2O + [Zn(ImH)_3(L4)]^{+} \quad (7)$$

$$[Zn(ImH)_3(OH_2)]^{2+} + L5^- \rightarrow H_2O + [Zn(ImH)_3(L5)]^{+} \quad (8)$$

$$[Zn(ImH)_3(OH_2)]^{2+} + CH_3S^- \rightarrow H_2O + [Zn(ImH)_3(CH_3S)]^+ \quad (9)$$

$$[Zn(ImH)_3(OH_2)]^{2+} + CH_3SH \rightarrow H_2O + [Zn(ImH)_3(CH_3SH)]^{2+} \quad (10)$$

$$[Zn(ImH)_3(OH_2)]^{2+} + L6 \rightarrow H_2O + [Zn(ImH)_3(L6)]^{2+} \quad (11)$$

This set of reactions includes several ligands not investigated in the binding mode study. They include methylthiolate (CH_3S^-), neutral methanethiol (CH_3SH), and the 2-thiazolyl analogue of L1[9] (L6). We include methylthiolate as a reference point and the other ligands for comparison.

As shown in Table 2, the binding affinity of the catalytic Zn ion complex for the ZBG ligand decreases in the order CH_3S^- > $L3^-$ > $L4^-$ > $L5^-$ > $L1^-$ > $L2^-$ ≫ L2 > L1 > L6 > CH_3SH. These data show that the gas-phase reactions, 2−11, fall into two groups, those with anionic ZBGs and those with neutral ZBGs. The anionic ligand−water exchange reactions are characterized by a large free-energy release (−162.2 to −178.8 kcal/mol) ostensibly due in part to the strong Coulombic attraction between the oppositely charged metal and ligand ions. The magnitude of ΔG_{exch} is significantly less for the neutral ligand−water exchange reactions but is still substantially negative for all but the methanethiol ligand (eq 10); its binding free energy is quite small suggesting much weaker coordination than CH_3S^-. This result agrees with previous molecular dynamics simulations, DFT calculations, and experimental findings that argue for the protonation of the coordinated cysteine thiolate of the MMP prodomain being an important step in the activation of MMPs by release of the prodomain.[30]

Cysteine side chains are generally considered to be deprotonated when coordinated to zinc centers.[22,23] Our calculations show that reaction 9 is favorable with a free-energy yield of 178.8 kcal/mol, greater than all other ligand reactions in the list. Cheng et al.[33] have performed similar DFT calculations on the thiolate−water exchange reaction and have obtained ΔG of −180.3 kcal/mol, which is in good agreement with our calculated value. Their most exothermic (spontaneous) reaction was obtained with the hydroxamate ZBG ($\Delta G = -193.2$ kcal/mol), while their least spontaneous reaction was with the hypophosphite ZBG ($\Delta G = -174.4$ kcal/mol).

The results in Table 2 show that ΔG_{exch} for the thiolate form of the mercaptoketone is more negative than that for either of the mercapto alcohol thiolates, with all being more positive than methylthiolate. These results are consistent with the experimental results of Campbell and co-workers who have shown mercaptoketone compounds have greater inhibitory activity than mercapto alcohols toward several MMPs.[17,18] Furthermore, these results are consistent with the interpretation of Puerta et al. that mercaptoketones have greater activity than the mercapto alcohols by virtue of the former having bidentate Zn coordination while the latter exhibit monodentate coordination when bound to $ZnTp^{Me,Ph}$.[19]

Although it is not known whether the mercaptoketone or mercapto alcohol ligands bind to the catalytic zinc in their neutral or anionic forms, evidence suggests that they bind as thiolates. The Zn−S distances from crystal structures of model complexes based on the $Tp^{Me,Ph}$ ligand are 2.23 Å for four-coordinate Zn(II) and 2.27 Å for the five-coordinate complexes. The Zn−S distances in proMMP-3[34] and thiol-based-inhibitor-bound MMP-8[35] are 2.18 and 2.23 Å, respectively. The small molecule structures are clearly thiolates and the MMP structures contain thiols that have thiolate character by virtue of their H-bond donation to the carboxylate side chain of the conserved Glu in the catalytic site. In contrast, the Zn−S distance is substantially longer, at 2.50 Å, in proMMP-2 (E404A),[36] wherein the catalytic Glu residue is mutated to Ala. Furthermore, we have calculated the structure of $[Zn(ImH)_3(HSCH_3)]^{2+}$ using the same DFT methods described above. The Zn−S distance in this structure is 2.48 Å (cf. 2.25 Å for the $[Zn(ImH)_3(SCH_3)]^+$ analogue, structures not shown). Taken together, the long Zn−S bonds in the crystal structure of the (E404A) mutant of proMMP-2 and in the calculated $[Zn(ImH)_3(HSCH_3)]^{2+}$ structure suggest that, without the conserved Glu to serve as a H-bond acceptor in the catalytic site, the coordinated Cys sulfur is likely to be protonated. The catalytic zinc center is completely buried in the proMMPs. Whether a thiol-based inhibitor would remain protonated in the more solvent-exposed catalytic site of activated MMP-2 (E404A) is unclear. Nevertheless, the contrast between the long Zn−S bonds in thiol complexes and the short Zn−S bonds in thiolate complexes of the cataltyic Zn(II) in proMMP-3[34] and inhibited MMP-8[35] reveals the importance of the conserved catalytic Glu in modulating the strength of the Zn−ZBG bond. Moreover, the smaller K_i of the bidentate mercaptoketone suggests that thiolate character and chelation conspire to impart potent inibitory properties to these ZBGs.

If the imidazole-based ligands bind the catalytic zinc in their anionic forms, the $L1^-$ ligand is expected to exhibit greater inhibition than $L2^-$ by virtue of the former having a more negative free-energy change than the latter, −166.1 and −162.2 kcal/mol, respectively. However, while both anionic imidazole-based ligands have calculated zinc binding affinities less than thiolate or the anionic mercaptoketone, the affinity of $L1^-$ for zinc is similar to both mercapto alcohols, −166.1 versus −167.9 or −168.5 kcal/mol, which inhibit MMPs with IC_{50} values in the nM range.[17,18] If the imidazole-based ligands bind to the zinc active site in their neutral state, our calculations show that L2 is expected to bind significantly greater than L1 or L6, the thiazolyl-based ligand. This is consistent with the secondary amine being a stronger base than the acyclic imines.

3.3. Proton Dissociation Energies. Results presented in the previous section show that binding free energy of a ZBG and, therefore, its inhibitory efficacy[37] will depend on the protonation state of the Zn−ZBG complex. Upon replacement of the catalytic water molecule by the ZBG, there are three possible fates of the bound ZBG proton. One is that it is transferred within the active site to the conserved glutamate side chain. Another is that it leaves the active site and becomes solvated by bulk water. Finally, it may remain on the ZBG. To evaluate which of these fates is the most energetically favorable in general and for the ligands studied here, gas-phase proton dissociation energies (PDEs) have been determined for the ZBGs and Zn−ZBG complexes discussed above. All of the aqueous ZBGs investigated in this study are protonated (charge neutral) at physiological pH. Thus, the Zn−ZBG complex may lose a proton after formation. The contribution of Zn−ZBG deprotonation to the stability of the ZBG-bound enzyme depends on how the enzyme active site accommodates the proton.

Reactions 12 and 13 show generalized proton dissociation reactions for the ZBGs (LH) and the Zn−ZBG complexes ($[Zn(ImH)_3(LH)]^{2+}$).

$$LH \rightarrow L^- + H^+ \qquad \Delta G_{PDE} \quad (12)$$

$$[Zn(ImH)_3(LH)]^{2+} \rightarrow [Zn(ImH)_3L]^{+} + H^{+} \qquad \Delta G_{PDE} \tag{13}$$

Table 3 shows the calculated proton dissociation energies for several of the systems in this study. As expected, the neutral ligands become much easier to deprotonate (more acidic) when coordinated to the Lewis acidic Zn(II) center. These results are consistent with experimental observations, as well as other theoretical results, which show that ligand pK_a's decrease when bound to zinc.[14,38−40] This table also shows that proton dissociation energies of the free ligands in the gas phase descend in the order H_2O > CH_3SH > imidazole-based (L1, L2) ≈ mercapto alcohol (L5) ≈ mercaptoketone (L3). When bound to $[Zn(ImH)_3]^{2+}$, however, this order rearranges to imidazole-based > H_2O > mercaptoketone ≈ mercapto alcohol ≈ CH_3SH. This latter trend differs from an earlier study which showed the order to be imidazole > CH_3SH > H_2O.[14,38] In that study, the ligands were bound to divalent zinc, Zn(II)(*g*), having no other ligands bound. Hence, and not surprisingly,[21a] it is apparent from our results that additional zinc ligands exert significant influence on the relative proton dissociation energies of the ligands studied here.

On the basis of the short Zn−S bonds in proMMP-3[34] and thiol-inhibited MMP-8,[35] it has been suggested that the ligands are bound as thiolates. Similarities between the PDEs for the CH_3SH and the mercapto alcohols (L3 and L5, Table 3) make it reasonable to conclude that the mercaptoketone and mercapto alcohol inhibitors would also bind as thiolates. However, the situation with the imidazole-based ligands is less clear. Considering that the PDE of imidazole is significantly more positive than that of the thiols, and even H_2O, it is not obvious whether the imidazole-based ligands, L1 and L2, would bind to Zn in their anionic or neutral form. In the first of the studies by El Yazal et al.[14] on PDEs of Zn-bound ligands they postulated, on the basis of PDEs relative to *N*-methylacetamide, that imidazole may be deprotonated when coordinating to zinc in proteins. The following discussion addresses the question of where the dissociated proton goes.

The transfer of a ZBG proton to a proton acceptor in the active site would involve the carboxylate side chain of the conserved glutamate. The PDEs in Table 3 show that proton dissociation from Zn−ZBG costs between 175 and 213 kcal/mol. The energy yield from protonation of the carboxylate side chain of Glu is ∼345 kcal/mol.[14] Thus, Δ*G* for the proton transfer from Zn−ZBG to Glu is estimated at −132 to −170 kcal/mol. Two aspects of this proton-transfer reaction are noteworthy. To a first approximation, solvation energy of the proton does not contribute to the driving force of the transfer because both the proton donor and proton acceptor are within the inhibited active site and are inaccessible by water in the inhibitor-bound enzyme.[34,35] In other words, the aqueous pK_a's of the proton donor and acceptor are irrelevant to the transfer because the driving force depends on the *difference* in their intrinsic proton dissociation energies at the dielectric constant of the active site, which is generally considered to be about 3 or 4.[10b] Second, the proton transfer is favorable regardless of whether the donor is oriented toward the Glu side chain or not. If the donor is oriented toward the Glu acceptor, additional stabilization is realized from H-bonding between the bound ZBG and Glu. Such H-bonding interactions are apparent from crystal structures of many inhibited MMPs[3,42] and ADAM-17 (TNF-α converting enzyme, TACE).[43]

Transfer of a bound ZBG proton to the bulk solvent is also conceivable. In contrast to the intraprotein transfer discussed above, solvation energy of the proton would contribute to the driving force of this dissociation reaction. The free energy of solvation for aqueous H^+ is −264 kcal/mol,[44] which would result in a dissociation driving force of −50 to −90 kcal/mol. Although such a reaction is predicted to be spontaneous, it is less favorable than intrapocket transfer to the Glu residue. The last consideration is whether the Zn−ZBG complex could remain protonated. Given the large driving forces for proton transfer within or out of the catalytic site, it appears questionable whether the complex could remain protonated in the activated enzymes. The crystal structure of proMMP-2[36] suggests a long Zn−S bond in the Glu404Ala mutant. Even though the native proton acceptor is missing from this active site, the bound Cys appears to be H-bonded to the amide side chain of Asn104 from the prodomain. This interaction in addition to the active site being protected from solvent by the prodomain may provide a combination of thermodynamic and kinetic stabilization sufficient to keep the proton in the active site.

TABLE 3: Proton Dissociation Energies (ΔH_{298} LH → L^- + H^+) with and without $[Zn(ImH)_3]^{2+}$ Present[a]

system	LH	$[Zn(ImH)_3LH]^{2+}$
	RO-H	
OH_2	388.6	182.6
	(390.8 ± 0.4)[b]	
L5		186.7
	RS−H	
CH_3SH	355.5	176.8
	(359.0 ± 2.1)[b]	
L3	342.0	175.9
L5	343.1	179.6
	N−H (imidazole)	
L1	344.1	203.5
L2	347.3	212.6

[a] Energies are from B3LYP/6-31+G(d,p)//6−31(d) calculations and are given in kcal/mol. Experimental values are in parentheses. [b] Reference 41.

The results presented here were obtained assuming a medium having dielectric constant (∈) =1. While ∈ of the inhibited enzyme active site is unlikely to be near that of water (80), it is certainly greater than 1.[10b] The influence of this difference on the relative driving forces for the proton-transfer processes discussed above is not obvious. Investigations of these effects are ongoing.

4. Conclusions

We have investigated the binding modes of imidazole- and thiol-based zinc binding groups through application of DFT methods to an in vacuo model of the metzincin active sites, $[Zn(ImH)_3L]^{1,2+}$, where L = either an imidazole- or thiol-based ZBG. For the imidazole-based ZBGs, the binding mode depends on the protonation state. If the ZBG binds as a neutral ligand, the lowest energy model complex is four-coordinate and has an intraligand hydrogen bond, whereas the corresponding anions tend to form five-coordinate (or five-/four-coordinate for $L2^-$) complexes. All of the thiol-based ligands show either weak five-coordination with a long Zn−O bond or S-bound four-coordination. These latter binding modes are in general, albeit not complete, agreement with experimentally determined small molecule crystal structures.

In addition, on the basis of proton dissociation energies and free-energy changes for ligand−water exchange reactions, the mercaptoketone and mercapto alcohol ligands are likely to bind in their thiolate forms. In contrast, the binding free energies of imidazole-based ligands are strongly negative whether they are

neutral or anionic. The results of this study predict that the intrinsic affinities of the catalytic zinc center for the anionic ligands investigated herein decrease in the order $L3^- > L4^- \approx L5^- > L1^- > L2^-$. However, the intrinsic affinities differ by energies on the order of nonbonded electrostatic interactions, such as hydrogen bonds. Thus, with optimized nonbonded interactions between inhibitor and the enzyme active site, imidazole-based ligands, and possibly other chelating N_2 ligands, hold promise as effective zinc binding groups in the design of metzincin inhibitors.

Acknowledgment. The calculations reported herein were facilitated by access to the North Dakota Computational Chemistry and Biology Network (NIH RR-16471) and the North Dakota State University Center for High-performance Computing. The authors are grateful for access to these facilities. Funding from NCRR (P20 RR15566) is also gratefully acknowledged.

Supporting Information Available: Cartesian coordinates for the structures in Figures 4−10. This material is available free of charge via the Internet at http://pubs.acs.org.

References and Notes

(1) Overall, C. M.; Lopez-Otin, C. *Nature Rev. Cancer* **2002**, *2*, 657−672.

(2) Brinckerhoff, C. E.; Matrisian, L. M. *Nature Rev. Mol. Cell Biol.* **2002**, *3*, 207−214.

(3) Whittaker, M.; Floyd, C. D.; Brown, P.; Gering, A. J. H. *Chem. Rev.* **1999**, *99*, 2735−2776.

(4) Borkakoti, N. *Biochem. Soc. Trans.* **2004**, *32*, 17−20.

(5) Coussens, L. M.; Fingleton, B.; Matrisian, L. M. *Science* **2002**, *295*, 2387−2392.

(6) Wynn, R. L. *Gen. Dent.* **1999**, *47*, 19−22.

(7) Egeblad, M.; Werb, Z. *Nature Rev. Cancer* **2002**, *2*, 161−174.

(8) Miller, M. J. *Chem. Rev.* **1989**, *89*, 1563−1579.

(9) He, H.; Linder, D. P.; Rodgers, K. R.; Chakraborty, I.; Arif, A. M. *Inorg. Chem.* **2004**, *43*, 2392−2401.

(10) (a) Dudev, T.; Lin, Y-l.; Dudev, M.; Lim, C. *J. Am. Chem. Soc.* **2003**, *125*, 3168−3180. (b) Dudev, T.; Lim, C. *Chem. Rev.* **2003**, *103*, 773−787.

(11) Roe, R. R.; Pang, Y.-P. *J. Mol. Model.* **1999**, *5*, 134−140.

(12) Alberts, I. L.; Nadassy, K.; Wodak, S. J. *Protein Sci.* **1998**, *7*, 1700−1716.

(13) Lin, Y.-I.; Lim, C. *J. Am. Chem. Soc.* **2004**, *126*, 2602−2612.

(14) El Yazal, J.; Pang, Y.-P. *J. Phys. Chem. B* **1999**, *103*, 8773−8779.

(15) El Yazal, J.; Roe, R. R.; Pang, Y.-P. *J. Phys. Chem. B* **2000**, *104*, 6662−6667.

(16) Gervasio, F. L.; Schettino, V.; Mangani, S.; Krack, M.; Carloni, P.; Parrinello, M. *J. Phys. Chem. B* **2003**, *107*, 6886−6892.

(17) Campbell, D. A.; Xiao, X.-Y.; Harris, D.; Ida, S.; Mortezaei, R.; Ngu, K.; Shi, L.; Tien, D.; Wang, Y.; Navre, M.; Patel, D. V.; Sharr, M. A.; DiJoseph, J. F.; Killar, L. M.; Leone, C. L.; Levin, J. I.; Skotnicki, J. S. *Bioorg. Med. Chem. Lett.* **1998**, *8*, 1157−1162.

(18) Levin, J. I.; DiJoseph, J. F.; Killar, L. M.; Sharr, M. A.; Skotnicki, J. S.; Patel, D. V.; Xiao, X.-Y.; Shi, L.; Navre, M.; Campbell, D. A. *Bioorg. Med. Chem. Lett.* **1998**, *8*, 1163−1168.

(19) Puerta, D. T.; Cohen, S. M. *Inorg. Chem.* **2002**, *41*, 5075−5082.

(20) Puerta, D. T.; Schames, J. R.; Henchman, R. H.; McCammon, J. A.; Cohen, S. M. *Angew. Chem., Int. Ed.* **2003**, *42*, 3772−3774.

(21) (a) Parkin, G. *Chem. Rev.* **2004**, *104*, 699−768. (b) Vahenkamp, H. *Acc. Chem. Res.* **1999**, *32*, 589−596.

(22) Dudev, T.; Lim, C. *J. Am. Chem. Soc.* **2002**, *124*, 6759−6766.

(23) Ryde, U. *Eur. Biophys. J.* **1996**, *24*, 213−221.

(24) (a) Becke, A. D. *J. Chem. Phys.* **1993**, *98*, 5648−5652. (b) Lee, C. T.; Yang, W. T.; Parr, R. G. *Phys. Rev. B* **1988**, *37*, 785−789. (c) Stephens, P. J.; Devlin, F. J.; Chablowski, C. F.; Frisch, M. J. *J. Phys. Chem.* **1994**, *98*, 11623−11627.

(25) Ziegler, T. *Chem. Rev.* **1991**, *91*, 651−667.

(26) Siegbahn, P. E. M.; Blomberg, M. R. A. *Annu. Rev. Phys. Chem.* **1999**, *50*, 221−249.

(27) Babine, R. E.; Bender, S. L. *Chem. Rev.* **1997**, *97*, 1359−1472.

(28) Frisch, M. J.; Trucks, G. W.; Schlegel, H. B.; Scuseria, G. E.; Robb, M. A.; Cheeseman, J. R.; Zakrzewski, V. G.; Montgomery, J. A., Jr.; Stratmann, R. E.; Burant, J. C.; Dapprich, S.; Millam, J. M.; Daniels, A. D.; Kudin, K. N.; Strain, M. C.; Farkas, O.; Tomasi, J.; Barone, V.; Cossi, M.; Cammi, R.; Mennucci, B.; Pomelli, C.; Adamo, C.; Clifford, S.; Ochterski, J.; Petersson, G. A.; Ayala, P. Y.; Cui, Q.; Morokuma, K.; Rega, N.; Salvador, P.; Dannenberg, J. J.; Malick, D. K.; Rabuck, A. D.; Raghavachari, K.; Foresman, J. B.; Cioslowski, J.; Ortiz, J. V.; Baboul, A. G.; Stefanov, B. B.; Liu, G.; Liashenko, A.; Piskorz, P.; Komaromi, I.; Gomperts, R.; Martin, R. L.; Fox, D. J.; Keith, T.; Al-Laham, M. A.; Peng, C. Y.; Nanayakkara, A.; Challacombe, M.; Gill, P. M. W.; Johnson, B.; Chen, W.; Wong, M. W.; Andres, J. L.; Gonzalez, C.; Head-Gordon, M.; Replogle, E. S.; Pople, J. A. *Gaussian 98*, Revision A.11.4; Gaussian, Inc.: Pittsburgh, PA, 2002.

(29) (a) Raghavachari, K.; Trucks, G. W. *J. Chem. Phys.* **1989**, *91*, 1062−1065. (b) Wachters, A. J. H. *J. Chem. Phys.* **1970**, *52*, 1033−1036. (c) Hay, P. J. *J. Chem. Phys.* **1977**, *66*, 4377−4384.

(30) Kotra, L. P.; Cross, J. B.; Shimura, Y.; Fridman, R.; Schlegel, H. B.; Mobashery, S. *J. Am. Chem. Soc.* **2001**, *123*, 3108−3113.

(31) Hunter, E. P. L.; Lias, S. G. *J. Phys. Chem. Ref. Data* **1998**, *27*, 413−656.

(32) Addison, A. W.; Rao, T. N.; Reedijk, J.; van Rijn, J.; Verschoor, G. C. *J. Chem. Soc., Dalton Trans.* **1984**, 1349−1356.

(33) Cheng, F.; Zhang, R.; Luo, X.; Shen, J.; Li, X.; Gu, J.; Zhu, W.; Shen, J.; Sagi, I.; Ji, R.; Chen, K.; Jiang, H. *J. Phys. Chem. B* **2002**, *106*, 4552−4559.

(34) (a) Becker, J. W.; Marcy, A. I.; Rokosz, L. L.; Axel, M. G.; Burbaum, J. J.; Fitzgerald, P. M. D.; Cameron, P. M.; Esser, C. K.; Hagmann, W. K.; Hermes, J. D.; Springer, J. P. *Protein Sci.* **1995**, *4*, 1966−1976. (b) Gooley, P. R.; O'Connell, J. F.; Marcy, A. I.; Cuca, G. C.; Axel, M. G.; Caldwell, C. G.; Hagmann, W. K.; Becker, J. W. *J. Biomol. NMR* **1996**, *7*, 8−28.

(35) Grams, F.; Reinemer, P.; Powers, J. C.; Kleine, T.; Pieper, M.; Tschesche, H.; Guber, R.; Bode, W. *Eur. J. Biochem.* **1995**, *228*, 830−841.

(36) Morgunova, E.; Tuuttila, A.; Bergmann, U.; Isupov, M.; Lindqvist, Y.; Schneider, G.; Tryggvason, K. *Science* **1999**, *284*, 1667−1670.

(37) Puerta, D. T.; Lewis, J. A.; Cohen, S. M. *J. Am. Chem. Soc.* **2004**, *126*, 8388−8389.

(38) El Yazal, J.; Pang, Y.-P. *J. Phys. Chem. B* **2000**, *104*, 6499−6504.

(39) Lipscomb, W. N.; Strater, N. *Chem. Rev.* **1996**, *96*, 2372−2433.

(40) Cross, J. B.; Duca, J. S.; Kaminski, J. J.; Madison, V. S. *J. Am. Chem. Soc.* **2002**, *124*, 11004−11007.

(41) Bartmess, J. E.; Scott, J. A.; McIver, R. T., Jr. *J. Am. Chem. Soc.* **1979**, *101*, 6046−6056.

(42) Bode, W.; Fernandez-Catalan, C.; Tschesche, H.; Grams, F.; Nagase, H.; Maskos, K. *Cell. Mol. Life Sci.* **1999**, *55*, 639−652.

(43) Grams, F.; Reinemer, P.; Powers, J. C.; Kleine, T.; Pieper, M.; Tschesche, H.; Huber, R.; Bode, W. *Eur. J. Biochem.* **1995**, *228*, 830−841.

(44) Tissandier, M. D.; Cowen, K. A.; Feng, W. Y.; Gundlach, E.; Cohen, M. H.; Earharat, A. D.; Coe, J. V.; Tuttle, T. R., Jr. *J. Phys. Chem. A* **1998**, *102*, 7787−7794.